Overexpression of STARD3 attenuates oxidized LDL-induced oxidative stress and inflammation in retinal pigment epithelial cells

Almarhoun, Mohammad; Biswas, Lincoln; Alhasani, Reem Hasaballah; Wong, Aileen; Tchivelekete, Gabriel Mbuta; Zhou, Xinzhi; Patterson, Steven; Bartholomew, Chris; Shu, Xinhua

Published in:
Biochimica et Biophysica Acta (BBA) - Molecular and Cell Biology of Lipids

DOI:
10.1016/j.bbalip.2021.158927

Publication date:
2021

Document Version
Author accepted manuscript

Overexpression of STARD3 attenuates oxidized LDL-induced oxidative stress and inflammation in retinal pigment epithelial cells

Mohammad Almarhoun[1], Lincoln Biswas[1], Reem Hasaballah Alhasani[1,4], Aileen Wong[1], Gabriel Mbuta Tchivelekete[1], Xinzhi Zhou[1], Steven Paterson[1], Chris Bartholomew[1] , Xinhua Shu[1,2,3*]

1 Department of Biological and Biomedical Sciences, Glasgow Caledonian University, Glasgow G4 0BA, United Kingdom

2 Department of Vision Science, Glasgow Caledonian University, Glasgow G4 0BA, United Kingdom

3 School of Basic Medical Sciences, Shaoyang University, Shaoyang, Hunan 422000, P. R. China

4 Department of Biology, Faculty of Applied Science, Umm Al-Qura University, Makkah, Saudi Arabia

* Corresponding author: Xinhua.Shu@gcu.ac.uk

Abstract

Age-related macular degeneration (AMD) is the most common cause of visual disorder in aged people and may lead to complete blindness with ageing. The major clinical feature of AMD is the presence of cholesterol enriched deposits underneath the retinal pigment epithelium (RPE) cells. The deposits can induce oxidative stress and inflammation. It has been suggested that abnormal cholesterol homeostasis contributes to the pathogenesis of AMD. However, the functional role of defective cholesterol homeostasis in AMD remains elusive. STARD proteins are a family of proteins that contain a steroidogenic acute regulatory protein-related lipid transfer domain. There are fifteen STARD proteins in mammals and some, such as STARD3, are responsible for cholesterol trafficking. Previously there was no study of STARD proteins in retinal cholesterol metabolism and trafficking. Here we examined expression of the Stard3 gene in mouse retinal and RPE cells at ages of 2 and 20 months. We found that expression of *Stard 3* gene transcripts in both mouse RPE and retina was significantly decreased at age of 20 months when compared to that of age 2 months old. We created a stable ARPE-19 cell line overexpressing STARD3 and found this resulted in increased cholesterol efflux, reduced accumulation of intracellular oxidized LDL, increased antioxidant capacity and lower levels of inflammatory cytokines. The data suggested that STARD3 is a potential target for AMD through promoting the removal of intracellular cholesterol and slowing the disease progression.

Key words Age-related macular degeneration, STARD3, retinal pigment epithelial cells, cholesterol efflux, oxidized low density lipoprotein

1. Introduction

Age-related macular degeneration (AMD) is characterized by severe visual impairment of the central retina and a leading cause of blindness among aged people worldwide. It is predicted that the number of AMD patients will increase from 196 million by 2020 to 288 million by 2040 due to population ageing (Wong et al., 2014). AMD is a chronic retinal disease and can progress to neovascular (wet) AMD and geographic atrophy (dry AMD) at advanced stage. Wet AMD has new vessels grown from the choroid into the sub-retinal space, leading to the leakage of fluid, lipid or blood into the sub-retinal space. Clinically, wet AMD can present as haemorrhage, lipid exudates, pigment epithelial detachment or sub-retinal fluid (Bolin and Kang, 2012). Dry AMD is characterised as drusen formation (yellow-white spots) beneath the retinal pigment epithelium (RPE), Bruch's membrane thickening and abnormal architecture, and lipofuscin accumulation in the RPE; abnormal deposits are also formed in the subretinal space, called reticular pseudodrusen (Bolin and Kang, 2012). Analyses of AMD patient eye samples have shown both cholesterol and lipoprotein are accumulated in drusen, reticular pseudodrusen and Bruch's membrane, suggesting there is possibly a defect in cholesterol transport in photoreceptor/RPE/Bruch's membrane (Pikuleva and Curcio, 2014). It is supposed surplus cholesterol in peripheral tissue cells, e.g. the RPE, moves back to the liver via reverse cholesterol transport (RCT) (Ikonen, 2006). The components of the RCT pathway have been shown to express in human and mouse RPE and in a human RPE cell line, ARPE-19 (Duncan et al., 2009; Biswas et al., 2017; Storti et al., 2017; Zheng et al., 2012); while active cholesterol efflux is ~~shown to~~ present in human and mouse primary RPE and in ARPE-19 cells (Biswas et al., 2017; Ishida et al., 2006; Storti et al., 2017). Genome-wide association studies have demonstrated that genes involved in the RCT are link to AMD development (Burgess and Smith, 2017; DeAngelis et al., 2017; Yuan et al., 2018). Recently Storti et al. (2019) reported mice with RPE-specific knockout of the cholesterol efflux gene, *Abca1*, displayed AMD-like retinal phenotypes, including lipid accumulation in the RPE, increased inflammation, RPE and photoreceptor degeneration, and decreased visual function. These findings suggested the RCT pathway may play a

critical role in the pathogenesis of AMD. Therefore, promotion of the removal of RPE cholesterol may be an effective therapeutic strategy for the treatment of early AMD patients.

The steroidogenic acute regulatory proteins (StAR) belong to a family of proteins in mammals that are classified to fifteen various members, STARD1-STARD15 and are divided into six subfamilies. All members consist of the StAR-related lipid transfer (START) domain and are believed to play major roles in the transport and metabolism of lipids (Alpy and Tomasetto, 2005). The STARD1 subfamily contains cholesterol-specific binding proteins: STARD1 and STARD3. STARD1 is a mitochondrial protein and regulates steroidogenesis by delivering cholesterol from the mitochondrial outer membrane to the mitochondrial inner membrane, where cholesterol is converted to pregnenolone by cytochrome P450 enzymes (Clark and Stocco, 1995). STARD3 is located to the membrane of late endosomes and is responsible for cholesterol transport from late endosomes to the endoplasmic reticulum (ER) and mitochondria (Charman et al., 2010; Wilhelm et al., 2017). Depletion of STARD3 reduced cholesterol transported from late endosomes to mitochondria and decreased production of CYP11A1-catalysed pregnenolone in Chinese hamster ovary cells (Charman et al., 2010). Knockdown of STARD3 also affects actin-dependent late endosome dynamics and cholesterol transport (Hölttä-Vuori et al., 2005). Overexpression of STARD3 in breast cancer cells resulted in decreased total free cholesterol and alteration of cellular cholesterol distribution (Vassilev et al., 2015). Overexpression of STARD3 also caused higher production of mitochondrial superoxide, decreased mitochondrial membrane potential and ATP synthesis, and mitochondrial fragmentation in a human liver cancer cell line (HepG2) (Balboa et al., 2017). In addition, overexpression of STARD3 also enhances cholesterol efflux in human macrophages and rat hepatoma cells but not in rat insulinoma cells, suggesting STARD3 plays different roles in different organs (Borthwick et al., 2010; Pinto and Graham, 2016; Soffientini et al., 2014). STARD 3 is the only member of STARD family, which is enriched in macula and which binds Lutein (Li et al., 2011). High levels of Lutein in sera or in ocular tissues are associated with a reduced risk for AMD (Feng et al., 2019). However, the function of STARD3 in RPE cells has been not investigated.

In the current study, we examined STARD expression in mouse retina and established a STARD3 overexpressing cell line. We found STARD3 expression in the retina was significantly decreased in aged mice, overexpression of STARD3 in ARPE-19 cells enhanced cholesterol efflux, decreased uptake and accumulation of oxidized low density lipoprotein (oxLDL) and suppressed oxLDL-induced oxidative stress and inflammation.

2 Materials and methods

2.1 Set-up of a STARD3-overexpressing stable cell line

ARPE-19 cells were seeded at a density of 1X 10^5 cells per well in a 24-well plate with 0.5ml DMEM/F12 media and incubated overnight in an incubator at 37 °C with 5 % CO2. 500 ng FLAG-tagged STARD3 plasmid with pCMV6-Entry vector backbone (Cat. RC228357, OriGene Technologies, Inc., Rockville, USA), or pCMV6-Entry vector (Cat. PS100001, OriGene Technologies, Inc., Rockville, USA) were transfected into ARPE-19 cells using Lipofectamine-2000 (Cat. 11668- 027, Life technology) following the manufacturer's protocol. After incubation at 37°C for 48 hours, the media were removed. Media with G418 (1mg/ml) were added to kill non-resistant cells without integration of transfected plasmids. Media with G418 were replaced every 3 days. After 21 days, cells were colonised. These colonised cells were trypsinized and transferred into 6-well plates. Overexpression of STARD3 in individual colonies was verified by Western blotting with anti-FLAG antibody.

2.2 Treatment of oxidized low density lipoprotein (oxLDL) in ARPE-19 cells

ARPE-19 cells were seeded in 12-well plates and treated with oxLDL (200µg/ml) or fluorescence labelled oxLDL (Dil oxLDL, 10µg/ml) for 4 or 24 hours. Both oxLDL and Dil-oxLDL were purchased from Alfa Aesar (Cat. J65591 and J64164, respectively). Dil oxLDL treated cells were washed with PBS for three times, fixed with 4% Paraformaldehyde for 10 min at room temperature and then mounted with DAPI. The intracellular DiI OxLDL was visualized under a confocal microscope and quantified using the Image J software. oxLDL treated cells were collected and subject to biochemical analysis.

2.3 Measurement of cholesterol efflux

ARPE-19 cells were seeded on 12 well plates and labelled with [3H] cholesterol for 24 hours with 2% BSA in serum free culture media. Efflux was initiated by the addition of serum-free DMEM/ F12 consisting human apoAI (10 g/ml), apoE (10 mg/ml), HDL (20 mg/ml) or human serum (1%, v/v) for 24 hours. The media were collected and centrifuged for 10 minutes at 12,000 rpm to remove residual dead cells. 200µl of media were transferred into scintillation counter and radioactivities were counted. The cholesterol efflux was then calculated according to our previous description (Biswas et al., 2017).

2.4 Measurement of reactive oxygen species (ROS)

ROS production in control or STARD3 overexpressing cells exposed with or without oxLDL for 4 hours and 24 hours was detected using DCFH-DA Assay Kit (Cat. D6883, Sigma, UK) following the manufacture's guidance. The relative ROS level was represented as (fluorescence of treated cells/ fluorescence of untreated cells)×100%.

2.5 Quantitative real-time polymerase chain reaction (qRT-PCR)

All animal work was approved by the Animal Welfare and Ethical Review Body, University of Strathclyde (Project licence P8C815DC9). Retinas and RPE/choroid were collected from four male mice at each age point (2, 6, 12 and 20 months old). The samples of each age group were pooled together and homogenized. RNA was extracted using Tri Reagent (Cat. T9424, Sigma, UK) according to the manufacture's protocol. cDNA synthesis was performed using a High-Capacity cDNA Reverse Transcription Kit (Cat. 436814, Applied Biosystems, UK). The quantification of targeted expression was detected by qRT-PCR assay using a Platinum® SYBR® Green QPCR SuperMix-UDG w/ROX kit (Cat. 11744100, Invitrogen, UK). The sequences for primers used for qRT-PCR were listed in Table S1.

2.6 Western blotting

Cells and mouse tissues (retinas and RPE/choroid pooled from 4 male mice at age of 2 or 20 months) were lysed using lysis buffer and concentration of extracted protein was quantified using a Bradford assay. 50 µg of individual samples were separated by SDS-PAGE and transferred to nitrocellulose membrane. The membrane was blocked with 5% non-fat dried milk in Tris-buffered saline, 0.1%

Tween 20 (TBST), incubated with primary and secondary antibodies. Signals of targeted proteins were detected using the LICOR Odyssey FC Imaging System. The densities of targeting protein bands were measured by the Odyssey Fc Imager with Image Studio™ Software (https://www.licor.com/bio/odyssey-fc/). The intensity of target protein was normalized to the intensity of GAPDH to determine relative protein intensity.

2.7 Immunostaining

Cells were seeded on sterilized round coverslips in a 12-well plate. These cells were fixed with 100% methanol at -20°C for 5 minutes, washed 3 times with PBS and blocked with PBS containing 2% bovine serum albumin (BSA) for 30 minutes at room temperature. Cells were then incubated with anti-STARD3 antibody (Cat. ab3478, Abcam, 1:200 dilution) or anti-FLAG antibody (Cat. F1804, Sigma, 1:200 dilution) overnight at 4°C. Further, cells were washed with PBS for three times (5 minutes/each) and blocked with 2% sheep serum in 2% BSA/PBS for 30 minutes at room temperature. In addition, cells were incubated with secondary antibody (Alexa Fluor® Plus 488 goat anti-mouse IgG, Cat. A32723, 1:500 dilution or Alexa Fluor® Plus 488 goat anti-rabbit IgG, Cat. A32731, 1:500 dilution, Thermo Fisher Scientific) for 45 minutes at room temperature in dark. Cells were then washed 5 times with PBS and mounted using DAPI. Images were captured under confocal microscope.

Cryosections of eyes from 3 months old male mice were blocked by 2% BSA/PBS for 30 minutes at room temperature and incubated with anti-STARD3 antibody and anti-rhodopsin antibody (Cat. Ab98887, 1:200 dilution, Abcam) overnight at 4°C, follow by the procedures described above.

2.8 Oil red O staining

Cells were seeded on cover slips in 12-well plates and exposed to oxLDL for 4 and 24 hours. Cells were incubated with Propylene Glycol for 2 minutes then with Oil Red O solution (Cat. ab150678, Abcam) for 6 minutes. Further cells were exposed to 85% Propylene Glycol for 1 minute and rinsed with distilled water for 2 minutes twice. Finally, cells were incubated in haematoxylin for 2 minutes

and further rinsed with distilled water for three times. Intracellular stained lipids were imaged using an EVOS M5000 microscope.

2.9 Biochemical assays

Measurement of superoxide dismutase (SOD) and catalase (CAT) activity and quantification of glutathione (GSH) and malondialdehyde (MDA) were carried out using the OxiSelect Superoxide Dismutase Activity Assay Kit (Cat. STA-340), the catalase (CAT) Activity Assay kit (Cat. STA-341), the total glutathione (GSSG/GSH) assay kit (Cat. STA-312) and the total OxiSelect™ TBARS Assay Kit (Cat. STA-312), respectively, purchased from Cell Biolabs UK, according to the manufacture's guidance.

2.10 Enzyme-linked immunosorbent assay (ELISA)

Media from control and STARD3 over-expressing cells treated with or without oxLDL (200μg/ml) were collected. Secreted IL-1 and TNF-α in the media were detected using Human IL-1β Mini TMB ELISA Development Kit (Cat. 900-TM95) and Human TNF-α Mini TMB ELISA Development Kit (Cat. 900-M25), respectively, according to the manufacture's protocols.

2.11 Statistical analysis

Data were analysed using unpaired t-test or one-way ANOVA followed by Bonferroni multiple comparison test using GraphPad Prism version 7 software (https://www.graphpad.com/scientific-software/prism/) and presented as mean ±SEM. A minimum of three independent experiments in triplicate were performed for statistical analysis. P value less than 0.05 was considered significant. *p<0.05, **p<0.01 and ***p<0.001.

3 Results

3.1 Expression of STARD3 in mouse retinas

Previous studies demonstrated STARD3 protein was expressed in human retinas and RPE/choroid and mouse RPE/choroid but not mouse retina (Li et al., 2011). We also examined the expression of STARD3 in mouse retinas using immunostaining with anti-rhodopsin and anti-STARD antibodies and found that STARD3 was predominantly localized to outer and inner segments of photorecepters, overlapping with rhodopsin staining. STARD3 were also localized to outer and inner plexiform layers

and ganglion cells. Weak signals were also detected in RPE (Figure 1A). We also examined expression of *Stard3* gene transcripts in mouse retina and RPE/choroid at age of 2, 6, 12 and 20 months by qRT-PCR. Stard3 mRNA levels in mouse retina and RPE/choroid was decreased with ageing, though there was no significantly difference in mice at 6 month old compared to that of mice at age of two months; there was significantly decreased expression in mouse retina and RPE/choroid at age of 12 and 20 months (Figure 1B). STARD3 protein level in the retina and RPE/choroid of mice at age of 2 and 20 months was also examined by Western blotting. We found that STARD3 protein was markedly lower in aged mouse retinas (Figure 1C). However, STARD3 protein was undetectable in the RPE by Western blotting (data not shown), possibly due to its expression at low level.

3.2 Overexpression of STARD3 in ARPE-19 cells

ARPE-19 cells were transfected with empty vector (pCMV6) and STARD3 plasmid (pCMV6-STARD3) and stable cell lines were selected using G418 screening. Human STARD3 was fused with a FLAG tag at the C terminal. To confirm overexpression of STARD3 protein, we used Western blotting to examine STARD3 protein level using anti-STARD3 and anti-Flag tag antibodies. The anti-STARD3 antibody detected both native STARD3 and FLAG-tagged STARD3; the anti-FLAG antibody only detected overexpressed STARD3. STARD3 was expressed in control cells; however, the stable cell line transfected with pCMV6-STARD3 had higher STARD3 expression (Figure 2). Overexpression of STARD3 protein was also detected by immunostaining using anti-STARD3 and anti-FLAG antibodies. Stronger fluorescent signals were detected with anti-STARD3 antibody in the stable cell line which contained native and overexpressed STARD3 when compared to control cells containing native STARD3 protein only (Figure S1).

3.3 Overexpression of STARD3 increased cholesterol efflux in ARPE-19 cells

Overexpression of STARD3 in macrophages enhanced cholesterol efflux and upregulated ABCA1 expression (Borthwick et al., 2010). We also examined whether overexpression of STARD3 affected cholesterol efflux in ARPE-19 cells. Under basal condition, there was no significant difference for cholesterol efflux between STARD3-overexpressing and control cells. In the presence of HLD and

human serum (HS), there is significantly increased cholesterol efflux in STARD3-overexpressing cells when compared to control cells ($p<0.0001$). However, cholesterol efflux to ApoA1 was not significantly changed in STARD3-overexpressing cells (Figure 3).

Our early work showed the mitochondrial translocator protein, TSPO, mediated cholesterol efflux in RPE cells (Biswas et al., 2017). Though STARD3 is responsible for transporting cholesterol from endosome to mitochondria, its relation with TSPO has not been investigated. We measured TSPO and STARD3 expression by qRT-PCR and Western blotting and found that STARD3-overexpressing cells had significantly increased TSPO expression at mRNA and protein level compared to that of control cells (Figures 4A, S2A). In TSPO knockout cells, whose cholesterol efflux is defective (Biswas et al., 2017), expression of STARD3 was notably lower than that of control cells (Figures 4B, S2B).

3.4 Overexpression of STARD3 decreased the uptake and accumulation of cholesterol

Since overexpression of STARD3 promoted cholesterol efflux, we examined whether STARD3 overexpression affects oxLDL uptake and accumulation. Both control and STARD3-overexpressing cells were exposed to fluorescence labelled oxLDL (Dil oxLDL) for 4 hours (uptake) or 24 hours (accumulation). Images were taken under confocal microscopy and fluorescence signals were quantified using Image J software. Results showed uptake of oxLDL was significantly lower in STARD3-overexpressing cells when compared to control cells; similarly, intracellular accumulation of oxLDL was markedly reduced in STARD3-overexpressed cells when compared to control cells (Figure 5).

Oil Red O staining is a commonly used method to detect neutral lipid and lipid droplets. Control and STARD3-overexpressed cells were fed with oxLDLL for 4 and 24 hours then stained with oil Red O. Intracellular lipid accumulation was significantly reduced in STARD3-overexpressed cells with oxLDL treatment for 4 and 24 hours when compared to control cells (Figure 6).

3.5 Overexpression of STARD3 reduced production of reactive oxygen species (ROS) and increased antioxidant capacity

OxLDL exposure is known to induce ROS production (Biswas et al., 2017). We also examined ROS production in control and STARD3-overexpressed cells with or without exposure to oxLDL. ROS production is significantly increased in control cells treated with oxLDL for 4 and 24 hours when compared to control cells without treatment. However, the STARD3 overexpressed cells treated with oxLDL for 4 and 24 hours had significantly lower levels of ROS when compared to control cells receiving similar treatment (Figure 7A).

OxLDL can induce oxidative stress and reduce antioxidant capacity. Control and STARD3-overexpressed cells were treated with oxLDL for 24 hours. Superoxide dismutase (SOD) activity was significantly increased by 129% in STARD3-overexpressed cells when compared to control cells with the same treatment; similarly, the activity of catalase (CAT) was significantly raised by 245% when compared to control cells (Figure 7B).

Glutathione (GSH) is an important antioxidant, which protects cells from reactive oxygen species (ROS) caused damage. GSH levels in STARD3-overexpressed cells were significantly increased 860% when compared to control cells (Figure 7B). Malondialdehyde (MDA) is a biomarker for lipid peroxidation. MDA was markedly decreased by 63% in STARD3-overexpressed cells when compared to control cells (Figure 7B).

3.6 Overexpression of STARD3 decreased secretion of inflammatory cytokines

We also examined expression of inflammatory cytokines (IL-1β and TNF-α) in control and STARD3-overexpressing cells. Both control and STARD3-overexpressing cells without oxLDL treatment had similar levels of IL-1β at 4 and 24 hours. However, IL-1 β secretion was significantly reduced in STARD3-overexpressing cells when compared to control cells incubated with oxLDL for 4 and 24 hours (Figure 8A). The level of TNF-α was not different between control and STARD3-overexpressing cells without oxLDL feeding for 4 and 24 hours. TNFα was only significantly decreased in STARD3-overexpressed cells when compared to control cells exposed to oxLDL for 24 hours (Figure 8B).

4. Discussion

STARD1 and STARD3 belong to the same subfamily of STARD proteins with 37% identity and 50% similarity of amino acids in the START domain (Alpy and Tomasetto, 2005). STARD1 transfers cholesterol from the endoplasmic reticulum (ER) to mitochondria and STARD3 transfers cholesterol from late endosomes to mitochondria. STARD1 associates with voltage-dependent anion channel (VDAC), TSPO, acyl coenzyme A-binding domain containing 3 (ACBD3) and the regulatory subunit RIof PKA (PKAIα) to form a multiprotein complex which is in charge of cholesterol trafficking (Liu et al., 2006). Elustondo et al postulate that STARDs also forms a multiprotein complex with VDAC and TSPO to mediate the transport of cholesterol from late endosomes to mitochondria (Elustondo et al., 2017). STARD3 interacts with vesicle-associated membrane protein-associated protein (VAP) family members (VAP-A, VAP-B and MOSPD3, motile sperm domain-containing protein2), facilitating the movement of cholesterol from endosomes to ER, where STARD1 delivers cholesterol to mitochondria (Alp et al., 2013; Mattia et al., 2020; Wilhelm et al., 2017). TSPO is responsible for transporting cholesterol from the outer mitochondrial membrane (OMM) to the inner mitochondrial membrane (IMM), where cholesterol is catalysed to oxysterols by CYP27A1 in non-steroidogenic cells (Rone et al., 2009). Oxysterols activate the liver X receptor (LXR) pathway and promote cholesterol efflux. Overexpression of STARD1 or STARD3 has been shown to enhance cholesterol efflux in macrophages (Borthwick et al., 2010; Taylor et al., 2010). In the current study we also demonstrated that overexpression of STARD3 resulted in a significant increase in cholesterol efflux to HDL and human serum (HS) (Figure 3). TSPO controls the import of STARD1 to IMM and mediates STARD1's activity (Rone et al., 2009). However, it is unclear whether TSPO cooperates with STARD3. Here we found a possible functional relationship between TSPO and STARD3 in RPE cells, since overexpression of STARD3 upregulated TSPO expression and loss of TSPO decreased STARD3 expression (Figure 4). Since overexpression of STARD1 or STARD3 upregulated cholesterol trafficking gene expression and facilitated lipid biosynthesis in non-retinal cells (Borthwick et al., 2010; Taylor et al., 2010), it is worth investigating whether overexpression of STARD3 has an impact on expression of cholesterol trafficking and metabolism genes in RPE cells.

Defects in cholesterol efflux by loss of TSPO increased uptake and accumulation of oxLDL in RPE cells (Biswas et al., 2017). Enhanced cholesterol efflux by TSPO ligands reduced oxLDL uptake and accumulation in choroidal endothelial cells (Biswas et al., 2018). Here we also found overexpression of STARD3 decreased uptake and accumulation of oxLDL in RPE cells and lowered intracellular neutral lipids (Figure 5). These results are compatible with a previous study that demonstrated a STARD3 (ΔSTART-STARD3) mutant leads to increased cholesterol accumulation in CHO cells and limits late endosomal trafficking (Zhang et al., 2002). Another study reported that the level of sterol ester storage was increased in Stard3 mutant mice fed a high fat diet (Kishida et al., 2004). OxLDL has been localized to the drusen and is supposed to induce oxidative stress, contributing to the progression of AMD (Yamada et al., 2008). Our previous work has shown that accumulation of oxLDL induces ROS production and decreases intracellular oxLDL resulting in less ROS production and elevated antioxidant capacity (Biswas et al., 2017, 2020). STARD3 overexpression significantly reduced ROS and MDA production, and increased SOD and CAT activity and the level of GSH in RPE cells exposed to oxLDL.

Raised ROS production by intracellular ox-LDL activates the NF-kB pathway and elevates the production of pro-inflammatory cytokines such as IL-1β and TNF α and IL-1β (Cominacini et al., 2000; Rodríguez and Larrayoz, 2010). OxLDL also mediates activation of the NLRP3 inflammasome, resulting in release of proinflammatory cytokines, IL-1β and IL-18 (Baldrighi et al., 2017). Early work demonstrated the oxLDL activated NLRP3 inflammasome in human primary fetal RPE and ARPE-19 cells (Gnanaguru et al., 2016). Our recent work showed oxLDL activated the NF-kB pathway (Biswas et al., 2020). OxLDL has been shown to induce secretion of pro-inflammatory cytokines in RPE cells (AnandBabu et al., 2019; Biswas et al., 2017; 2020). Our data showed that IL-1β and TNF-α levels were significantly decreased in STARD3 overexpressed cells when compared to control cells exposed to oxLDL. This is compatible with other studies which demonstrated oxidative stress increased inflammatory gene expression, including IL-1β, IL-8, TNF-α, VCAM-1 and INF-γ, and caused retinal disorders (Semeraro et al., 2015).

Cholesterol plays an important structural and metabolic role, which is required for cellular function. Cholesterol is also a key component to produce steroid hormones. Cellular level of cholesterol is well controlled, excess cholesterol in the RPE is removed via the reverse cholesterol transport to the liver for excretion or storage. Abnormal cholesterol homeostasis causes different types of diseases including AMD and atherosclerosis (Pikuleva and Curcio, 2014). Cholesterol is enriched in sub-RPE deposits of AMD patients and the Bruch's membrane also has enriched cholesterol, suggesting defects in reverse cholesterol transport. When aging, the Bruch membrane and the RPE cells become atrophied and degenerated, leading slowly to severe visual loss (Frankel and Sowka, 2011). Components of drusen, including cholesterol, have been shown to induce oxidative stress and inflammation. It will be a good therapeutic strategy to promote the removal of intracellular cholesterol by trafficking back to the liver and reduce drusen formation, which will slow disease progression in AMD patients. STARD3 overexpression enhanced cholesterol removal in RPE cells suggests it may be a therapeutic target for AMD. Further studies in animal models to address the functional roles of STARD3 are required.

In conclusion, overexpression of STARD3 enhanced cholesterol efflux, reduced intracellular accumulation of cholesterol, suppressed ROS production, increased antioxidant capacity and inhibited inflammation. Overexpression of STARD3 in RPE cells or development of ligands enhancing STARD3 function may be an effective strategy to treat AMD patients.

Author Contributions X.S. conceived the concept. M.A., L.B, R.H.A., A.W., G.M.T, and X.Z carried out the experiments. M.A., X.Z. and X.S. analysed the data. S.P. C.B. and X.S. drafted the manuscript.

Funding: This work was supported by a PhD scholarship from Kuwait Government, the Rosetrees Trust (M160, M160-F1, M160-F2), National Eye Research Centre (SAC037), Tenovus Scotland (S20-02) and the Lotus Scholarship Program of Hunan Province (2019). X.S. is a visiting Professor to Shaoyang University.

Conflicts of Interest: No conflict of interest needs to be declared.

References

Alpy, F. and Tomasetto, C., 2005. Give lipids a START: the StAR-related lipid transfer (START) domain in mammals. Journal of cell science, 118(13), pp.2791-2801.

AnandBabu, K., Sen, P. and Angayarkanni, N., 2019. Oxidized LDL, homocysteine, homocysteine thiolactone and advanced glycation end products act as pro-oxidant metabolites inducing cytokine release, macrophage infiltration and pro-angiogenic effect in ARPE-19 cells. PloS one, 14(5), p.e0216899.

Baldrighi, M., Mallat, Z. and Li, X., 2017. NLRP3 inflammasome pathways in atherosclerosis. Atherosclerosis, 267, pp.127-138.

Biswas, L., Zhou, X., Dhillon, B., Graham, A., Shu, X., 2017. Retinal pigment epithelium cholesterol efflux mediated by the18kDa translocator protein, TSPO, a potential target for treating age-related macular degeneration. Hum. Mol. Genet. 26, 4327-4339.

Balboa, E., Castro, J., Pinochet, M.J., Cancino, G.I., Matías, N., Sáez, P.J., Martínez, A., Álvarez, A.R., Garcia Ruiz, C., Fernandez-Checa, J.C. and Zanlungo, S., 2017. MLN64 induces mitochondrial dysfunction associated with increased mitochondrial cholesterol content. Redox biology, 12, pp.274-284.

Bolin X., and Kang L. (2012). Today and Future of Age-Related Macular Degeneration. ISRN Ophthalmology, 2012, 480212.

Borthwick, F., Allen, A.M., Taylor, J.M. and Graham, A., 2010. Overexpression of STARD3 in human monocyte/macrophages induces an anti-atherogenic lipid phenotype. Clinical Science, 119(7), pp.265-272.

Burgess, S. and Smith, G.D., 2017. Mendelian randomization implicates high-density lipoprotein cholesterol–associated mechanisms in etiology of age-related macular degeneration. Ophthalmology, 124(8), pp.1165-1174.

385 Charman, M., Kennedy, B.E., Osborne, N. and Karten, B., 2010. MLN64 mediates egress of
386 cholesterol from endosomes to mitochondria in the absence of functional Niemann-Pick Type C1
387 protein. Journal of lipid research, 51(5), pp.1023-1034.
388 Clark, B.J. and Stocco, D.M., 1995. Expression of the steroidogenic acute regulatory (StAR) protein: a
389 novel LH-induced mitochondrial protein required for the acute regulation of steroidogenesis in
390 mouse Leydig tumor cells. *Endocrine research*, *21*(1-2), pp.243-257.
391 Cominacini, L., Pasini, A.F., Garbin, U., Davoli, A., Tosetti, M.L., Campagnola, M., Rigoni, A., Pastorino,
392 A.M., Cascio, V.L. and Sawamura, T., 2000. Oxidized low density lipoprotein (ox-LDL) binding to ox-
393 LDL receptor-1 in endothelial cells induces the activation of NF-κB through an increased production
394 of intracellular reactive oxygen species. Journal of Biological Chemistry, 275(17), pp.12633-12638.
395 DeAngelis, M.M., Owen, L.A., Morrison, M.A., Morgan, D.J., Li, M., Shakoor, A., Vitale, A., Iyengar, S.,
396 Stambolian, D., Kim, I.K., Farrer, L.A., 2017. Genetics of age-related macular degeneration (AMD).
397 Hum. Mol. Genet. 26(R1), R45-R50.
398 Duncan, K.G., Hosseini, K., Bailey, K.R., Yang, H., Lowe, R.J., Matthes, M.T., Kane, J.P., LaVail, M.M.,
399 Schwartz, D.M. and Duncan, J.L., 2009. Expression of reverse cholesterol transport proteins ATP-
400 binding cassette A1 (ABCA1) and scavenger receptor BI (SR-BI) in the retina and retinal pigment
401 epithelium. British Journal of Ophthalmology, 93(8), pp.1116-1120.
402 Elustondo, P., Martin, L.A. and Karten, B., 2017. Mitochondrial cholesterol import. *Biochimica et*
403 *Biophysica Acta (BBA)-Molecular and Cell Biology of Lipids*, *1862*(1), pp.90-101.
404 Feng, L., Nie, K., Jiang, H. and Fan, W., 2019. Effects of lutein supplementation in age-related macular
405 degeneration. *PloS one*, *14*(12), p.e0227048.
406 Frankel, S., and Sowka, J. (2011). Neovascular age-related macular degeneration therapy confirmed.
407 Optometry - Journal of the American Optometric Association, 82(10), 598.
408 Gnanaguru, G., Choi, A.R., Amarnani, D. and D'Amore, P.A., 2016. Oxidized lipoprotein uptake
409 through the CD36 receptor activates the NLRP3 inflammasome in human retinal pigment epithelial
410 cells. Investigative ophthalmology & visual science, 57(11), pp.4704-4712.

411 Hölttä-Vuori, M., Alpy, F., Tanhuanpää, K., Jokitalo, E., Mutka, A.L. and Ikonen, E., 2005. MLN64 is
412 involved in actin-mediated dynamics of late endocytic organelles. Molecular biology of the cell, 16(8),
413 pp.3873-3886.
414 Ikonen, E. (2006). Mechanisms for cellular cholesterol transport: defects and human disease. Physiol.
415 Rev. 86, 1237–1261.
416 Ishida, B.Y., Duncan, K.G., Bailey, K.R., Kane, J.P. and Schwartz, D.M., 2006. High density lipoprotein
417 mediated lipid efflux from retinal pigment epithelial cells in culture. British Journal of Ophthalmology,
418 90(5), pp.616-620.
419 Kishida, T., Kostetskii, I., Zhang, Z., Martinez, F., Liu, P., Walkley, S.U., Dwyer, N.K., Blanchette-Mackie,
420 E.J., Radice, G.L. and Strauss, J.F., 2004. Targeted mutation of the MLN64 START domain causes only
421 modest alterations in cellular sterol metabolism. Journal of Biological Chemistry, 279(18), pp.19276-
422 19285.
423 Li, B., Vachali, P., Frederick, J.M. and Bernstein, P.S., 2011. Identification of StARD3 as a lutein-
424 binding protein in the macula of the primate retina. Biochemistry, 50(13), pp.2541-2549.
425 Liu, J., Rone, M.B. and Papadopoulos, V., 2006. Protein-protein interactions mediate mitochondrial
426 cholesterol transport and steroid biosynthesis. *Journal of Biological Chemistry*, *281*(50), pp.38879-
427 38893.
428 Pikuleva, I.A., Curcio, C.A., 2014. Cholesterol in the retina: the best is yet to come. Prog. Retin. Eye
429 Res. 41, 64-89.
430 Pinto, J.B. and Graham, A., 2016. The role of endosomal cholesterol trafficking protein, StAR-related
431 lipid transfer domain 3 (StarD3/MLN64), in BRIN-BD11 insulinoma cells. Protein & cell, 7(11), pp.833-
432 838.
433 Rodríguez, I.R. and Larrayoz, I.M., 2010. Cholesterol oxidation in the retina: implications of 7KCh
434 formation in chronic inflammation and age-related macular degeneration. Journal of lipid research,
435 51(10), pp.2847-2862.

436 Rone, M.B., Fan, J. and Papadopoulos, V., 2009. Cholesterol transport in steroid biosynthesis: role of
437 protein–protein interactions and implications in disease states. Biochimica et Biophysica Acta (BBA)-
438 Molecular and Cell Biology of Lipids, 1791(7), pp.646-658.
439 Semeraro, F., Cancarini, A., Rezzola, S., Romano, M.R. and Costagliola, C., 2015. Diabetic retinopathy:
440 vascular and inflammatory disease. Journal of diabetes research, 2015,582060
441 Soffientini, U., Caridis, A.M., Dolan, S. and Graham, A., 2014. Intracellular cholesterol transporters
442 and modulation of hepatic lipid metabolism: implications for diabetic dyslipidaemia and steatosis.
443 Biochimica et Biophysica Acta (BBA)-Molecular and Cell Biology of Lipids, 1841(10), pp.1372-1382.
444 Storti, F., Klee, K., Todorova, V., Steiner, R., Othman, A., van der Velde-Visser, S., Samardzija, M.,
445 Meneau, I., Barben, M., Karademir, D. and Pauzuolyte, V., 2019. Impaired ABCA1/ABCG1-mediated
446 lipid efflux in the mouse retinal pigment epithelium (RPE) leads to retinal degeneration. Elife, 8,
447 p.e45100.
448 Storti, F., Raphael, G., Griesser, V., Klee, K., Drawnel, F., Willburger, C., Scholz, R., Langmann, T., von
449 Eckardstein, A., Fingerle, J., Grimm, C., Maugeais, C., 2017. Regulated efflux of photoreceptor outer
450 segment-derived cholesterol by human RPE cells. Exp. Eye Res. 165, 65-77.
451 Taylor, J.M., Borthwick, F., Bartholomew, C. and Graham, A., 2010. Overexpression of steroidogenic
452 acute regulatory protein increases macrophage cholesterol efflux to apolipoprotein AI.
453 Cardiovascular research, 86(3), pp.526-534.
454 Vassilev, B., Sihto, H., Li, S., Hölttä-Vuori, M., Ilola, J., Lundin, J., Isola, J., Kellokumpu-Lehtinen, P.L.,
455 Joensuu, H. and Ikonen, E., 2015. Elevated levels of StAR-related lipid transfer protein 3 alter
456 cholesterol balance and adhesiveness of breast cancer cells: potential mechanisms contributing to
457 progression of HER2-positive breast cancers. The American journal of pathology, 185(4), pp.987-
458 1000.
459 Wilhelm, L.P., Wendling, C., Védie, B., Kobayashi, T., Chenard, M.P., Tomasetto, C., Drin, G. and Alpy,
460 F., 2017. STARD 3 mediates endoplasmic reticulum-to-endosome cholesterol transport at membrane
461 contact sites. The EMBO journal, 36(10), pp.1412-1433.

Wong, W.L., Su, X., Li, X., Cheung, C.M., Klein, R., Cheng, C.Y., Wong, T.Y., 2014. Global prevalence of age-related macular degeneration and disease burden projection for 2020 and 2040: a systematic review and meta-analysis. Lancet Glob. Health, 2, e106-116.

Yamada, Y., Tian, J., Yang, Y., Cutler, R.G., Wu, T., Telljohann, R.S., Mattson, M.P. and Handa, J.T., 2008. Oxidized low density lipoproteins induce a pathologic response by retinal pigmented epithelial cells. Journal of neurochemistry, 105(4), pp.1187-1197.

Yuan, M.Z., Han, R.A., Zhang, C.X., Chen, Y.X., 2018. Association of genes in the high-density lipoprotein metabolic pathway with polypoidal choroidal vasculopathy in Asian population: a systematic review and meta-analysis. J. Ophthalmol. 2018, 9538671.

Zhang, M., Liu, P., Dwyer, N.K., Christenson, L.K., Fujimoto, T., Martinez, F., Comly, M., Hanover, J.A., Blanchette-Mackie, E.J. and Strauss, J.F., 2002. MLN64 mediates mobilization of lysosomal cholesterol to steroidogenic mitochondria. Journal of Biological Chemistry, 277(36), pp.33300-33310.

Zheng, W., Reem, R.E., Omarova, S., Huang, S., DiPatre, P.L., Charvet, C.D., Curcio, C.A., Pikuleva, I.A., 2012. Spatial distribution of the pathways of cholesterol homeostasis in human retina. PLoS One 7, e37926.

Figures and legends

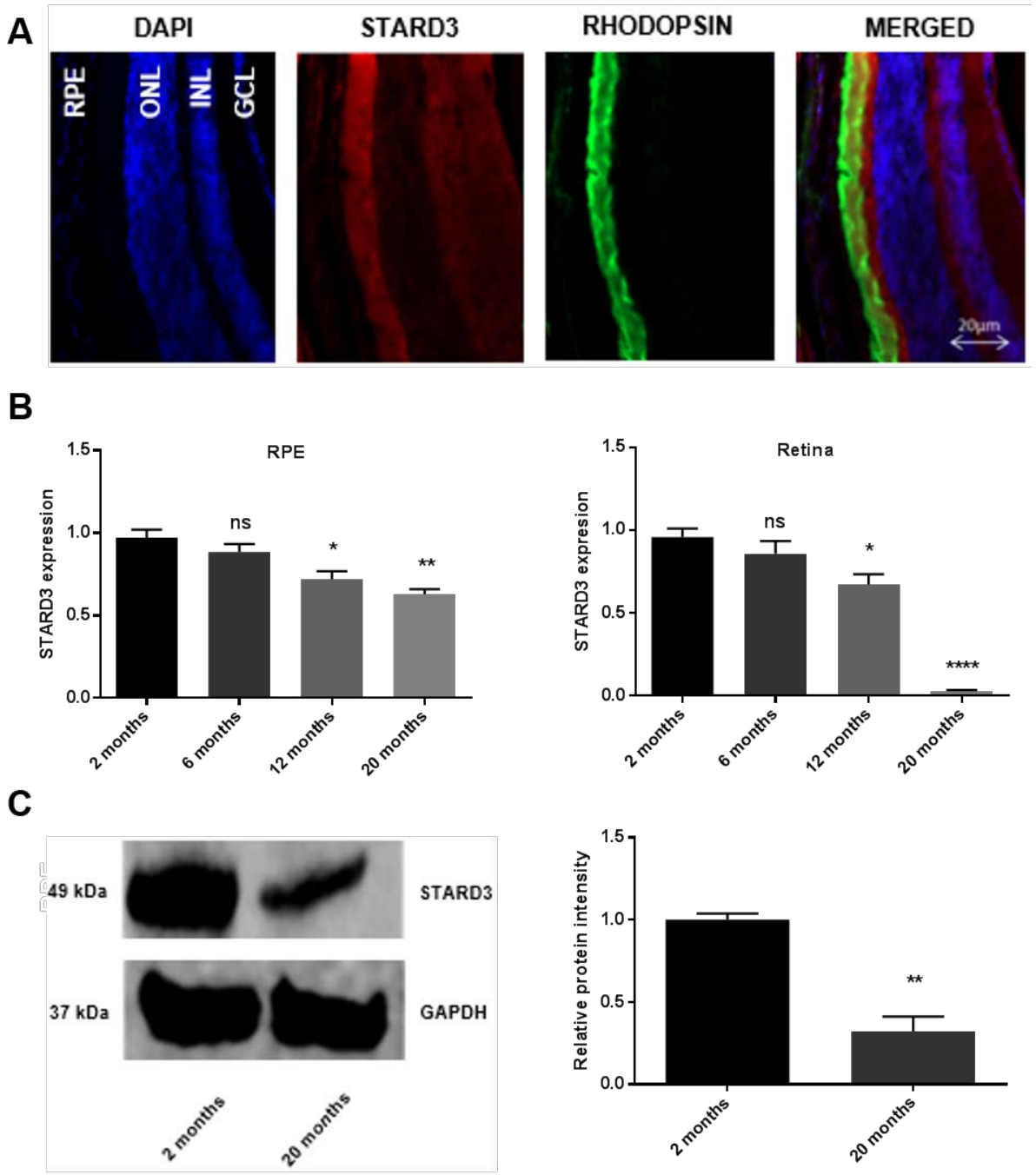

Figure 1 Stard3 expression in mouse retina and RPE. (A) Immunolocalization of STARD3 in mouse retina. Two-month old mouse eye sections were immune stained with an STARD3 antibody for STARD3 expression and DAPI for labelling nuclei. (B) Retinas and RPE/choroid were dissected from four male mice at age of 2, 6, 12 and 20 months. The samples at each age point were pooled together. RNAs were extracted and cDNAs were synthesized. mRNA levels of *Stard3* in the retina and

RPE/choroid were measured by qRT-PCR (n=4). Data was analysed by one-way ANOVA followed by Bonferroni multiple comparison test. (C) Retinas were dissected from four male mice at age of 2 or 20 months and pooled together. Proteins were extracted from the retinal samples using Tissue Extraction Buffer. STARD3 protein was detected by Western blotting and quantified by LI-COR Image Studio Software. Data were analysed by unpaired t-test followed by Bonferoni post hoc test and presented as mean ±SEM. GCL, ganglion cell layer; INL, inner nuclear layer; ONL, outer nuclear layer; RPE, retinal pigment epithelial cells. ns, no significance; *P<0.05, **p<0.01, ****p<0.0001.

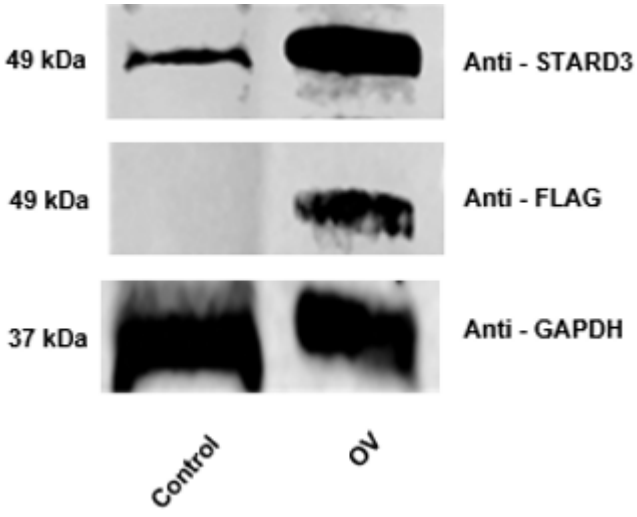

Figure 2 Overexpression of STARD3 protein was detected by Western blot with anti-STARD antibody and anti-FLAG antibody respectively. OV, STARD3-overexpressing cells.

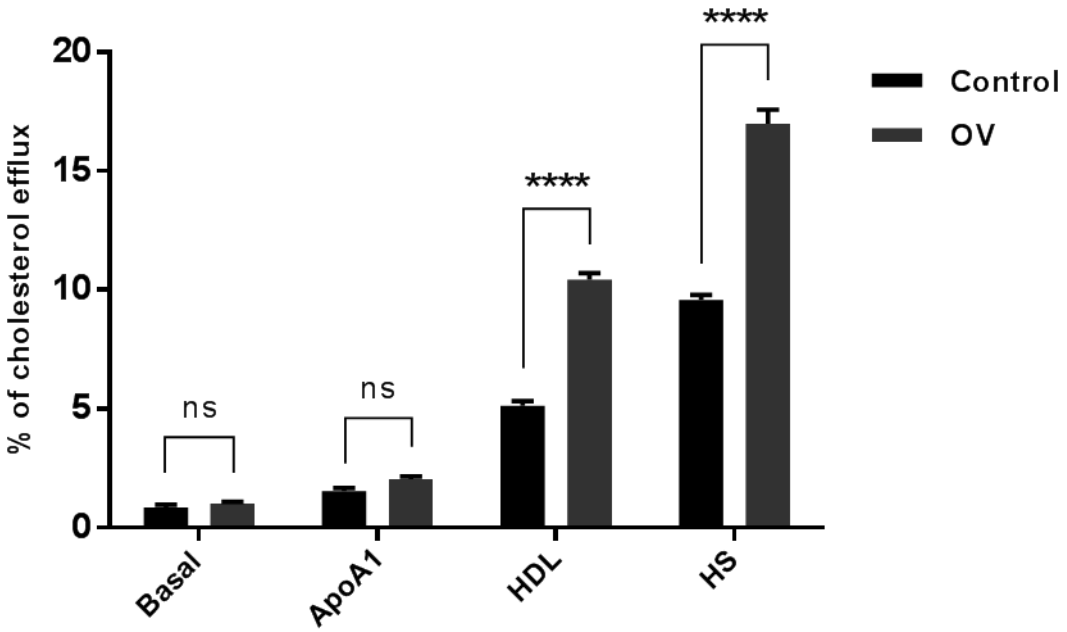

507

508 **Figure 3** Comparison of cholesterol efflux to ApoA1, HDL and human serum (HS) between cells with

509 overexpression of STARD3 (OV) and control cells (transfected with empty vector, pCMV6). Data were

510 Data were analysed by unpaired t-test with Bonferoni post hoc test and presented as mean ±SEM

511 (n=5). Ns, no significance, ****P<0.0001.

512

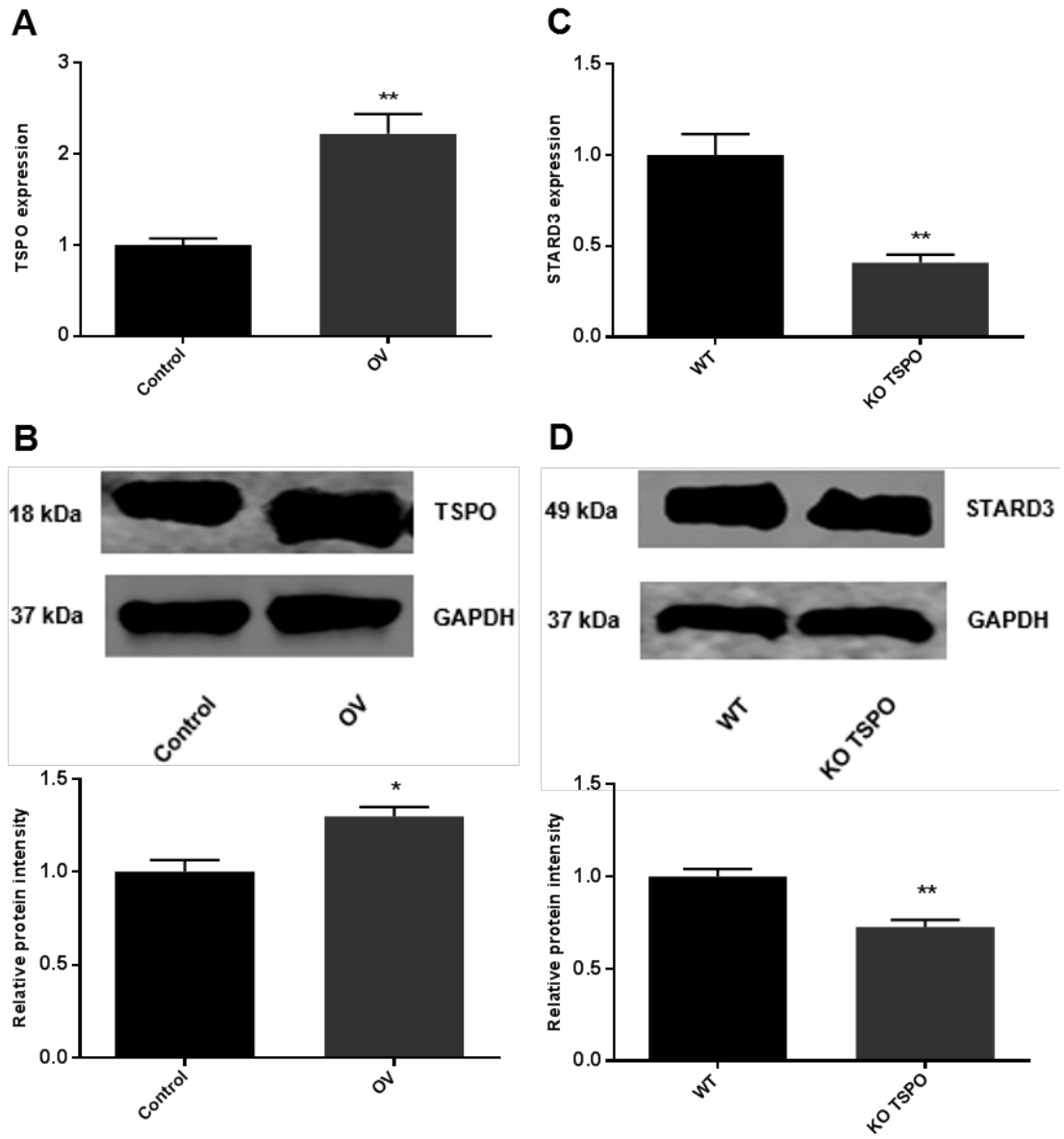

513

514 **Figure 4** Overexpression of STARD3 upregulated TSPO expression. (A) TSPO mRNA in control and
515 STARD3-overexpressing cells was detected by qRT-PCR. The data was analysed by unpaired t-test
516 followed by Bonferroni post hoc test and presented as mean ±SEM (n=4). (B) TSPO protein in control
517 and STARD-overexpressing cells was detected by Western blotting and quantified using LI-COR
518 Image Studio Software. The data was analysed by unpaired t-test followed by Bonferoni post hoc
519 test and presented as mean ±SEM (n=3). (C) STARD3 mRNA in wildtype and TSPO knockout cells.
520 The data was analysed by unpaired t-test followed by Bonferroni post hoc test and presented as
521 mean ±SEM (n=4). (D) STARD3 protein in wildtype and TSPO knockout cells was examined by

Western blotting and quantified by LI-COR Image Studio Software. The data was analysed by unpaired t-test followed by Bonferoni post hoc test and presented as mean ±SEM (n=3). OV: STARD3-overexpressing cells; KO TSPO, TSPO knockout cells. *p<0.05; **p<0.01.

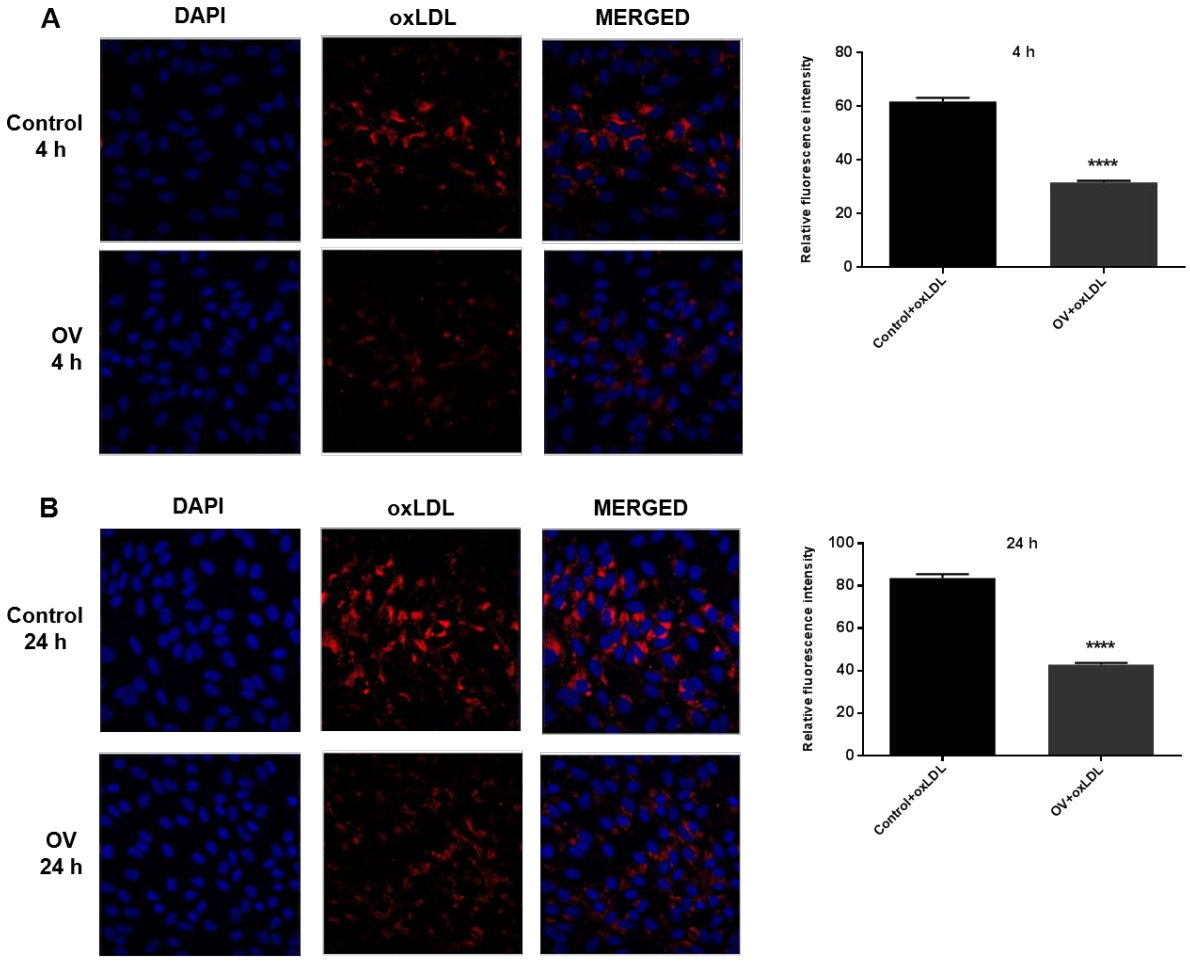

Figure 5 Uptake (A) and accumulation (B) of oxLDL in control and STARD3-overexpressing cells exposed to Dil oxLDL for 4 hours and 24 hours, respectively. Images were taken under confocal microscopy and fluorescent signals of intracellular oxLDL were quantified using Image J software and calculated the corrected total cell fluorescence (CTCF = Integrated Density – (Area of selected cell X Mean fluorescence of background readings)). The data was analysed by unpaired t-test followed by Bonferroni test and presented as mean ±SEM (n=5). OV, STARD3-verexpressing cells. Data were presented as mean±SEM. ****p<0.0001.

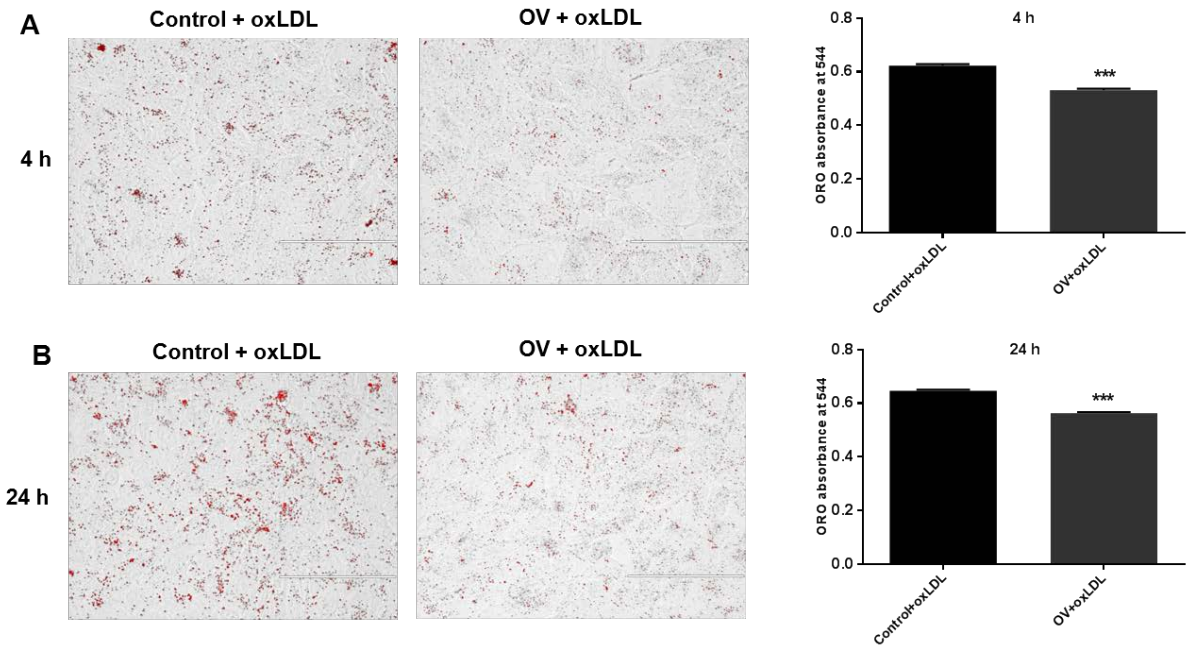

535

536 **Figure 6** The oil Red O (ORO) staining showed intracellular lipid droplets n control and STARD3-
537 overexpressing cells incubated with oxLDL for 4 hours (A) and 24 house (B). Images were taken
538 under light microscopy. After staining, lipid droplets were extracted with isopropanol and measured
539 using spectrometry at the absorbance of 544 nm and the data was analysed by unpaired t-test
540 followed by Bonferroni post hoc test and presented as mean ±SEM (n=4). OV: STARD3
541 overexpressing cells. Data were presented as mean±SEM. ***P<0.001.

542

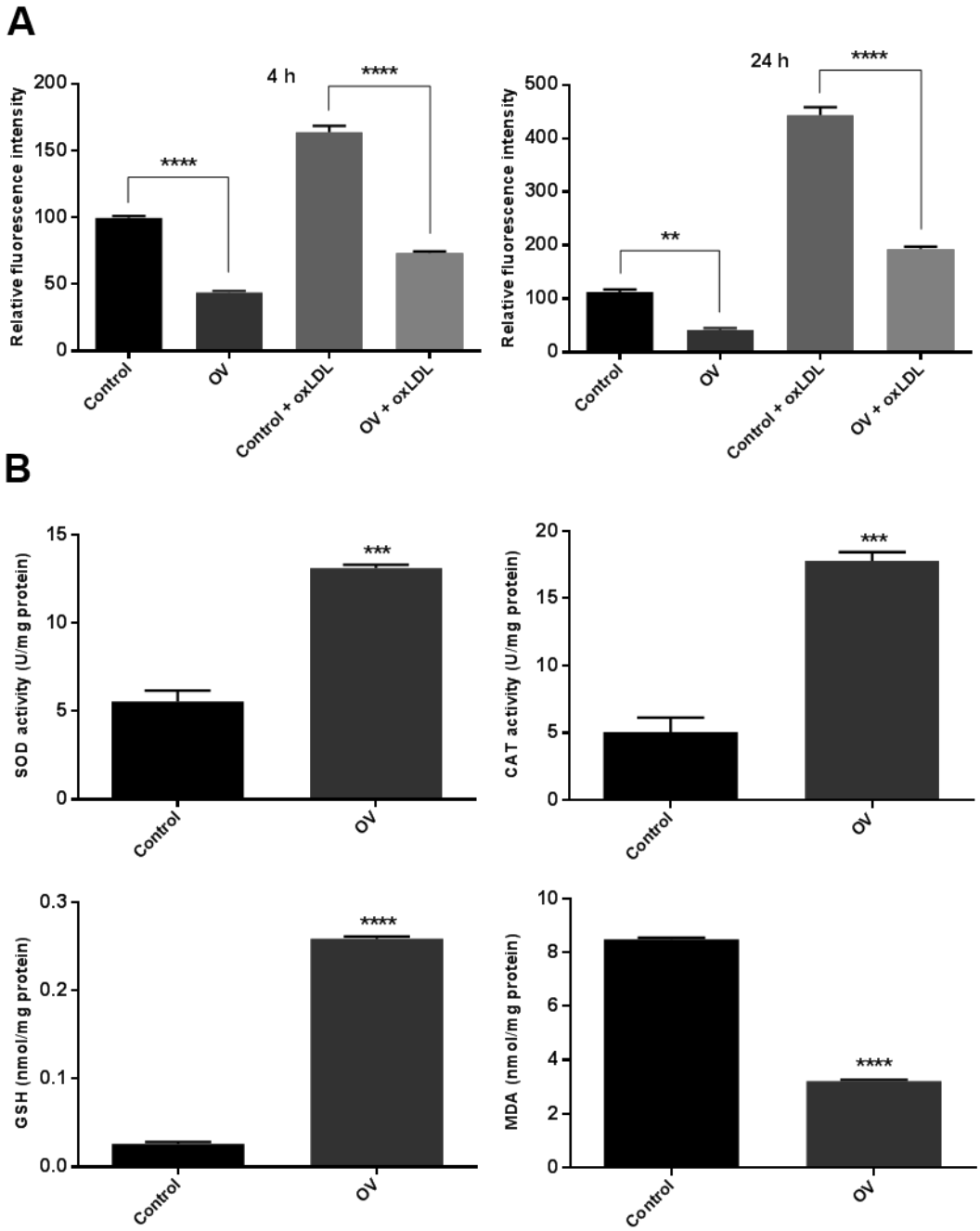

Figure 7 (A) Production of reactive oxygen species (ROS) in control and STARD3-overexpressing cells treated with/without oxLDL for 4 hours and 24 hours. (B) The effects of overexpressed STARD3 on activities of superoxide dismutase (SOD) and catalase (CAT) and on production of glutathione (GSH) and malonialdehyde (MDA) in control and STARD3-overexpressing cells (OV) fed with oxLDL for 24 hours. All the data were analysed by unpaired t-test followed by Bonferroni test and presented as mean ±SEM (n=5). **P<0.01; ***p<0.001; ****p<0.0001.

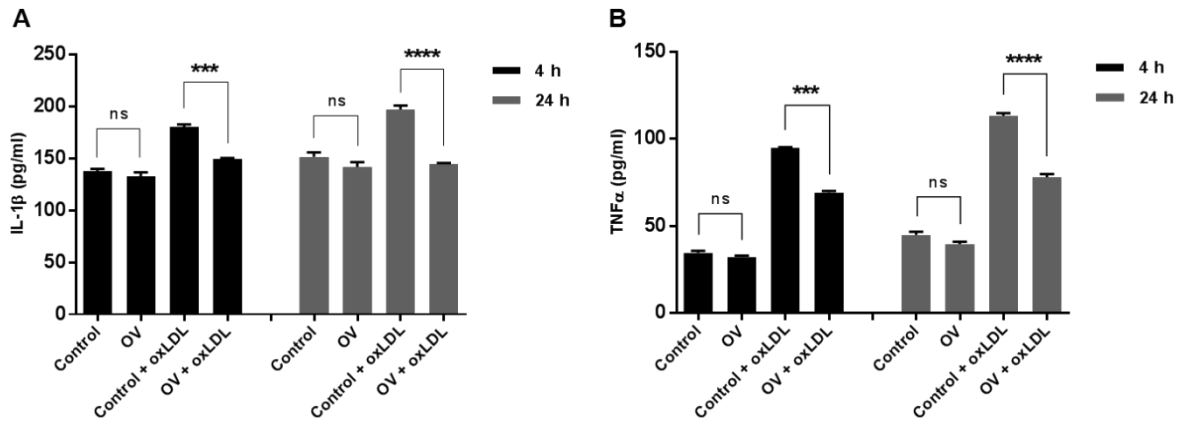

Figure 8 Overexpressed STARD3 decreased production of proinflammatory cytokines in LDL-exposed RPE cells. IL-1β (A) and TNFα (B) in control and STARD3-overexpressing cells treated with/without oxLDL for 4 hours and 24 hours were measured by ELISA. All the data were analysed by unpaired t-test followed by Bonferroni post hoc test and presented as mean ±SEM (n=5). OV: STARD3-overexpressing cells. Ns, no significance; ****P